How hydrophobic drying forces impact the kinetics of molecular recognition

Jagannath Mondal, Joseph A. Morrone, and B. J. Berne*
Department of Chemistry, Columbia University, New York, NY 10027

A model of protein-ligand binding kinetics in which slow solvent dynamics results from hydrophobic drying transitions is investigated. Molecular dynamics simulations show that solvent in the receptor pocket can fluctuate between wet and dry states with lifetimes in each state that are long enough for the extraction of a separable potential of mean force and wet-to-dry transitions. We introduce a Diffusive Surface Hopping Model that is represented by a two-dimensional Markovian master equation. One dimension is the standard reaction coordinate, the ligand-pocket separation, and the other is the solvent state in the region between ligand and binding pocket which specifies whether it is wet or dry. In our model, the ligand diffuses on a dynamic free energy surface which undergoes kinetic transitions between the wet and dry states. The model yields good agreement with results from explicit solvent molecular dynamics simulation and an improved description of the kinetics of hydrophobic assembly. Furthermore, it is consistent with a "non-Markovian Brownian theory" for the ligand-pocket separation coordinate alone.

I. INTRODUCTION

Recent theoretical work has shown that the displacement of water by drug molecules is important in the thermodynamics and kinetics of ligand—enzyme binding [1–3]. The kinetics of drug docking are known to be a key metric for lead optimization [4]. In the present work, we explore the kinetic motifs of hydrophobic association on ligand binding. This is achieved by the development of a simple model for hydrophobic association that is compared with explicit solvent molecular dynamics simulations.

One of the signature features of hydrophobic assembly is the observation of a dewetting transition [5–9]. Drying behavior has been found to play an important role in protein self-assembly and the behavior of nano-confined water [10, 11]. The present paper draws on our extensive work on the role of molecular-scale hydrodynamics in hydrophobic collapse [12, 13] where we showed that when the attraction between water and two associating nanoscale objects is weak, assembly proceeds via a drying transition in the inter-solute region. This transition is characterized by large peaks in the rel-

ative translational friction coefficient that correspond to large and slow solvent fluctuations. The slow relaxation times exhibited by water undergoing dewetting transitions suggest that resulting non-Markovian effects may prove to be a crucial element in a full description of the assembly kinetics.

We presently extend our earlier investigations to a model of a spherical ligand docking in a concave cavity. The model is similar to one investigated in a series of papers by McCammon and co-workers [14, 15], but altered to describe the assembly of a nanoscale ligand. This alteration facilitates the study of a large-scale drying transition. We investigate the molecularscale hydrodynamic effects and the kinetic rate constants for binding and develop a theoretical framework to describe hydrophobic assembly which couples the diffusive reaction coordinate (the separation) to transitions between "wet" and "dry" states which are defined by a coarse-grained solvent occupancy in the binding pocket. This model is conceptually similar to the surface hopping algorithm employed in non-adiabatic quantum dynamics [16], and thus we call it the diffusive surface hopping model (DSHM). We show how the model reproduces the effect of drying fluctuations that are evidenced in an ensemble of explicit solvent molec-

^{*} bb8@columbia.edu

ular dynamics assembly trajectories. We compare different kinetic schemes with the results of all-atom molecular dynamics.

In very recent work, Setny, et al. [17] have computed the hydrodynamic profile for the ligand binding model that originated in Ref. 14. It was found that enhanced and slowed hydration fluctuations engender a slow down in the ligand dynamics, in agreement with our results on model plates and spheres [12, 13]. work also reported a shift in the spatial hydrodynamic effect that was attributed to non-Markovian effects. We find a related behavior in our study and show that it is resolved by use of the DSHM. In this way, the theoretical framework that is presently introduced yields a coarse-grained dynamical scheme that improves upon the description obtained from Smoluchowski (Brownian) dynamics when slow solvent motions are important.

II. COARSE GRAINED DESCRIPTIONS OF HYDROPHOBIC ASSEMBLY

Ligand binding kinetics is often described by the Smoluchowski Equation:

$$\frac{\partial p(q,t)}{\partial t} = \frac{\partial}{\partial q} D(q) \left(\frac{\partial}{\partial q} - \beta \bar{F}(q) \right) p(q,t) \left(1 \right)$$

where q is the separation between ligand and receptor, p(q,t) is the time-dependent probability distribution function, $\bar{F}(q) = -\partial W(q)/\partial q$ is the mean force, W(q) is the potential of mean force, $D(q) = k_b T/\zeta(q)$ is the spatially dependent diffusion coefficient, and $\zeta(q)$ is the friction coefficient. This is a Markovian equation and is valid if solvent fluctuations are very fast compared to solute motions. The spatial dependence of the diffusion coefficient arises from hydrodynamic interactions (HI) between the receptor and ligand. $\bar{F}(q)$ and the $\zeta(q)$ may be computed from MD [12, 13]. Eq. (1) was tested in our previous work but we observed very slow solvent fluctuations at and around the drying transition between hydrophobic plates (or spheres). Indeed the autocorrelation function of the solvent force along q exhibited prominent long time tails, indicating that non-Markovian effects should be important. In such cases solvent degrees of freedom must be included in describing hydrophobic assembly[10, 18]. We now develop a theory that is applicable to the ligand-receptor model. It includes a coarse grained description of the solvent as an explicit degree of freedom of the dynamics, and involves a two dimensional Smoluchowski equation, which although Markovian, yields a non-Markovian expression for p(q,t) in place of Eq. (1), when the solvent degree of freedom is projected out.

We propose a two dimensional model where one coordinate is the diffusive coordinate q (the separation between receptor and ligand), and the other is a discrete state variable s = w or d, indicating whether the binding pocket is wet or dry, respectively. This model has state dependent diffusion coefficients, D(w,q) and D(d,q), evolves on state-dependent free energy surfaces, W(w,q) and W(d,q), and its state can change from wet to dry and from dry to wet by first order kinetics with rate constants also depending on q, namely $k(d \leftarrow w, q)$ and $k(w \leftarrow d, q)$ are the rate constants to transition from $w \to d$ and $d \to w$, respectively. This model is equivalent to a particle diffusing on a potential energy surface that can hop between two functional forms, one for the wet and one for dry states, with different spatially dependent diffusion constants on each surface. We call this the Diffusive Surface Hopping Model (DSHM). Such a scheme can be described by the following two differential equation for the time evolution of the probability density p(s,q,t):

$$\frac{\partial p(s,q,t)}{\partial t} = \frac{\partial}{\partial q} D(s,q) \left(\frac{\partial}{\partial q} - \beta \bar{F}(s,q) \right) p(s,q,t) -k(s' \leftarrow s,q) p(s,q,t) + k(s \leftarrow s',q) p(s',q,t) ,$$
(2)

where $\bar{F}(s,q) = -\partial_q W(s,q)$. One equation where s = w and s' = d is paired to one corresponding to s = d and s' = w. In this way, the diffusion dynamics is coupled to transitions between the surfaces.

DSHM reduces to Eq. (1) when the hopping rate between surfaces is fast compared to the

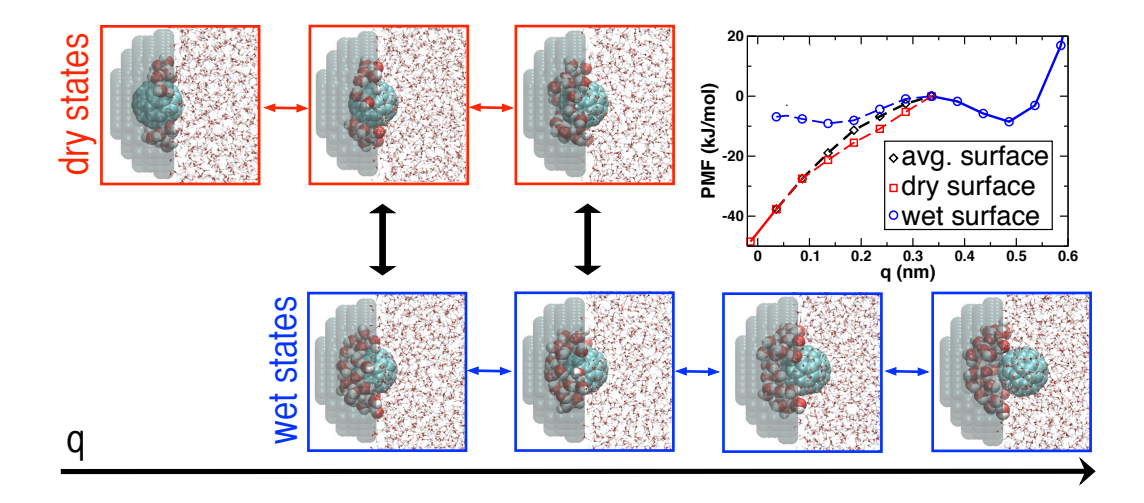


FIG. 1. Schematic for the Markovian master equation analysis that is presently employed. Transitions amongst wet states (blue framed snapshots) and dry states (red framed snapshots) occur along q. Transitions between wet and dry states may occur in the dewetting region at fixed q. In the upper-right panel the potential of mean force is plotted on the wet surface (blue line) and dry surface (red line). In the region of drying, two of the models presently considered evolve along an averaged surface (black dashed line). Snapshots are rendered with VMD [19].

rate of diffusion along q (see Appendix). This model is similar in spirit to one discussed in Ref. 20 where diffusing charged particles in an electric field can hop between two states with different diffusion coefficients and electric mobilities, with the hopping governed by first order chemical kinetics. However in this prior formulation, a treatment of the spatial dependence of the diffusion coefficients, electrical mobilities, and transition rates is ignored.

Application of Eq. (2) calls for specifying mean force and diffusion coefficient separately for both the wet and dry states as well as a set of transition rates between these states. The problem can be simplified for our receptor-ligand problem since transitions between wet and dry states only take place for separations in a narrow range (in the neighborhood of the critical distance for drying q_c). We assume that for large values of q only wet states are accessible and for small values of q only dry states are accessible. Then one need only consider transitions between surfaces in a specific "drying re-

gion." One can then discretize the continuous Smoluchowski dynamics [21], and place both Eq. (1) and Eq. (2) in the form of a Markovian Master Equation:

$$\frac{\partial p_i(t)}{\partial t} = R_{ij}p_j(t) , \qquad (3)$$

where the index i runs over all allowed states, and where q is represented on a grid. Eq. (2) describes evolution of two surfaces, both wet and dry. The detailed expressions for R_{ij} in the case of both one dimensional Smoluchowski (Brownian) dynamics and our two dimensional two surface representation are given in the Appendix, and a schematic depicting how transitions are made in two surface model is depicted in Fig. 1. Markovian Master Equations (Markov State models) can serve as an important tool to analyze conformational changes in biomolecules and extract kinetic information from molecular simulation [22], and have been also utilized to treat solvent degrees of freedom, including drying fluctuations in carbon nanotubes [23, 24].

The elements of the rate matrix \boldsymbol{R} given in Eq. (3) are obtained from a molecular dynamics simulation runs in explicit solvent where the ligand-pocket separation q is restrained to a set of values along the assembly path. The model ligand is a C60 fullerene and the pocket is an ellipsoidal hole carved from a hydrophobic wall. Further details are given in the Appendix.

III. RESULTS AND DISCUSSION

A. Average mean force and hydrodynamic profiles

The nature of the free energy surface and hydrodynamic interactions that the solute experiences depends intrinsically on the strength of the solute-water interaction. Vastly different behavior is exhibited in the case of very hydrophobic bodies where assembly is facilitated by drying as compared with more hydrophilic bodies where steric interactions engender the expulsion of water at small separations. We have computed the potential of mean force and hydrodynamic profile for the model pocket for three different strengths of solvent attraction. The interactions that describe the ligand are not varied. The weakest and intermediate interactions conform to the case of hydrophobic assembly driven by drying transitions, whereas the behavior of the strongly attractive pocket is dominated by steric ejections of water. The intermediate strength of attraction will be the focus of this work and discussion of the other two cases is presented in the Appendix.

Figs. 2B and 2D show how the number of water molecules in the first solvation shell of the ligand, N_{Ligand} and the number of pocket water molecules N_{Pocket} vary as a function of the reaction coordinate q for intermediate pocket-water attraction. As the ligand enters the pocket, the system undergoes a drying transition around $q_c = 0.186$ nm. As the ligand is rather hydrophilic, there is a free energy penalty associated with the stripping away of waters from the fullerene. There is also an observed maximum in the number of pocket water molecules

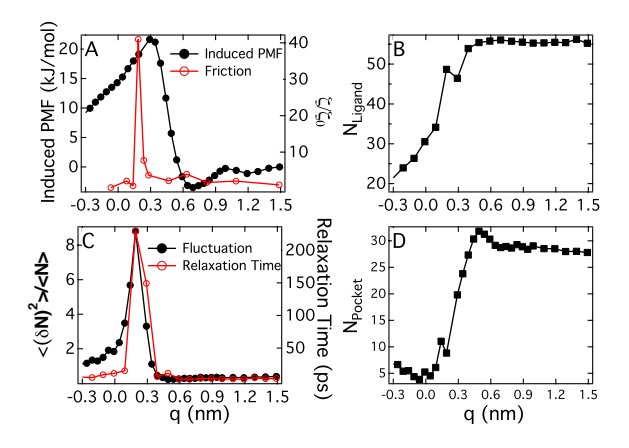


FIG. 2. Layout describing the correlations among various thermodynamic and hydrodynamic profiles as a function of ligand-pocket distance for intermediate-attractive pocket. (A) Comparison of the solvent-induced PMF (left scale) and friction profile(right scale), (B) ligand-water number profile, (C) Correlation of pocket-water fluctuation (left scale) and relaxation time (right scale), and (D) pocket-water number profile.

as the ligand approaches the cavity, owing to the intrusion of the ligand solvation shell into the pocket.

The solvent-induced potential of mean force and variation of the friction coefficient with separation q are plotted in Fig. 2A. Unlike our previous work where the friction coefficient was computed from the force-force autocorrelation function, [25], we presently utilize a technique that applies a harmonic restraint along the q-direction at several positions and probes the relaxation of the position autocorrelation function [26, 27]. The region of drying is associated with a large peak in the friction coefficient, $\zeta(q)$. The mean solvent induced force, is attractive near q_c . For the present system, barriers primarily arise from the desolvation of the ligand (see Fig. 2B).

Plotted in Fig. 2C are the solvent fluctuations and relaxation times in the binding pocket as a function of q. These properties have been found to yield trends relatable to those observed for

the profile of the friction coefficient in our previous works [12, 13], and this is also observed in the present work. It is seen that relaxation times greater than 200 ps are present in the cavity near the dewetting transition. As we will show later, this timescale is of the same order as the mean first passage time for the ligand to bind to the pocket starting from entry into the pocket. Such slow fluctuations indicate that the simple one dimensional Brownian dynamics approximation does not hold, and non-Markovian effects are significant.

B. Hydrophobic forces on wet and dry surfaces

A detailed characterization of the underlying solvent coordinate in the DSHM calls for a quantitative analysis of the dry and wet states observed in the dewetting region. The probability distribution and representative trajectory of the pocket water molecules are shown for $q=q_c$ in Fig. 3 (A) and (B). From the plot of the number of waters in the region between ligand and pocket versus time in panel A, one sees that the wet and dry states have sufficiently long survival times, and therefore various average properties for the wet and dry states can be determined.

To underline the importance of the slow fluctuations between wet and dry states at the dewetting transition, we plot the normalized position autocorrelation function of the total system in Fig. 3D and for the wet and dry states separately in Fig. 3C. One can see that the relaxation times of the correlation functions are markedly shorter when the states are considered separately. The friction coefficient in the wet and dry states may be estimated from the correlation function $\langle q(0)q(t)\rangle$ using the approach in Refs. [26, 27]. The friction in the wet state is close to the value found at large separations, whereas in the dry state it is approximately half of this. Therefore the pronounced hydrodynamic effect we observe at the drying transition in this and prior studies is shown to be due to slow transitions between the wet and dry states, and it is appealing to incorporate this as a sepa-

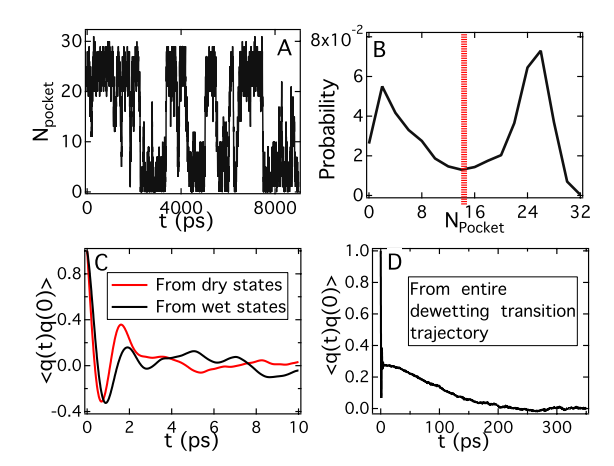


FIG. 3. (A) Representative trajectory exhibiting continuous fluctuations between wet and dry state at $q_c = 0.186$ nm. (B) The probability distribution of solvent occupancy in the pocket at q_c . Configurations to the left and right of the dashed red line are considered to be in "dry" or "wet" states, respectively. The normalized position autocorrelation function about $\langle q \rangle = q_c$ is plotted in the wet (black line) and dry (red line) states in panel (C) and the total autocorrelation function from which the friction coefficient at q_c is determined is plotted in panel (D). The long tail of the total correlation function is absent in the wet and dry state results, indicating that the large friction is associated with slow solvent fluctuations due to drying and wetting events.

rate slow collective variable, whereas other solvent degrees of freedom remain treatable in the Markovian limit. Indeed, this is the rationale behind the Diffusive Surface Hopping Model.

C. Constructing the Diffusive Surface Hopping Model

The parameterization of our Diffusive Surface Hopping Model (DSHM) draws from the underlying simulation results as obtained in the region of the drying transition. As evident from Eq. (2), the three main inputs necessary for DSHM are the mean force and diffusion coefficient along the two surfaces and the rate constants for transitions between wet and dry states. Here we will briefly outline only the salient features of how we construct the DSHM using simulation as the source of parameters. A detailed discussion of the parameterization is reserved for the Appendix.

The DSHM requires mean forces on the dry and wet surfaces. It consists of numerous wet and dry states set on a equally spaced grid along q. For the purpose of this model, a state is defined as dry if there are fewer than 15 water molecules in the pocket, and wet otherwise. We extract mean "dry" and "wet" forces by averaging over wet and dry configurations separately at each fixed q in the dewetting region. The resulting potentials of mean forces, which include the direct interactions of heavy bodies, that correspond to the wet and dry surfaces are plotted in Fig. 1.

Another crucial set of input parameters for DSHM are the rate constants for the transitions, wet \rightleftharpoons dry. Such transitions are only treated in the dewetting region. Only wet and dry states are considered at large and small separations, respectively. The matrix elements are estimated from the average dwell times in the wet state from MD simulations at fixed q. The reverse transitions are then estimated from the detailed balance condition and the equilibrium probabilities of being in a wet or dry state. The values of the inverse rate constants at the values of q considered are given in Table 1. The transition times are shown to become shorter as the bodies approach each other and fewer water molecules are displaced by the drying event. Recent work on the rate of drying [8, 9] finds that the activation free energy depends on distance through linear and quadratic terms which are related through macroscopic arguments to surface and line tensions. We find our present data set too sparse to elaborate on this finding. At small separations, we include two states on the wet surface for which the solvation state is dry for long times. The inclusion of such "transient wet" states, which may be visited as the ligand diffuses along q, place the kinetics of assembly predicted by the model in quantitative

TABLE I. The period of wet to dry transitions and equilibrium occupancy of wet and dry states. At small q, no occupancy is given as it is dominated by the dry state.

q	$k^{-1}(q,d \leftarrow w)$	$P_{\rm dry}$	$P_{\rm wet}$
0.036 nm	6.0 ps	_	_
$0.086~\mathrm{nm}$	20.0 ps	_	_
$0.136~\mathrm{nm}$	75.8 ps	0.74	0.26
$0.186~\mathrm{nm}$	193 ps	0.44	0.56
$0.236~\mathrm{nm}$	212 ps	0.29	0.71
$0.286~\mathrm{nm}$	276 ps	0.38	0.62
$0.336~\mathrm{nm}$	519 ps	0.17	0.83

agreement with molecular dynamics simulation.

The diffusion coefficient in the dewetting region is taken to be constant, albeit with different values on the wet and dry surfaces ($D_{\text{wet}} = D_{\text{dry}}/2 = 7.56 \times 10^{-4} \, \text{nm}^2/\text{ps}$). The value of D_{wet} is taken to be the diffusion constant for the ligand at large separations. In this way, the hydrodynamic effect in the dewetting region is subsumed into the wet-to-dry transitions which are an explicit degree of freedom of the dynamics given by Eq. 2. Outside this region, the diffusion coefficient is parameterized from the frictional profile (Fig. 2A).

D. Comparison of Diffusive Surface Hopping Model with other dynamical schemes

In order to directly compare the dynamics of the DSHM to explicit solvent molecular dynamics simulation and to one-dimensional Smoluchowski dynamics, we determine the time-dependent spatial distribution function, P(q,t), and the mean first passage times (MFPT) for assembly from MD simulations where the pocket is fixed and the ligand is free to move in the direction of q. To guarantee that the ligand cannot diffuse far from the binding site, a repulsive wall potential is added to the system. The resultant potential of mean force, including the repulsive wall, is depicted in Fig. 1. It is important to note that these simulations differ

from those from which the model parameters were determined, where q was fixed at different values.

Apart from comparing with MD simulations, it is also of interest to compare the two dimensional model (DSHM) to one-dimensional diffusion (Smoluchowski) dynamics on the average potential of mean force described by the Markovian master equation, Eq. (1) including either a position-dependent or a constant diffusion coefficient [21]. The diffusive dynamics occurs on the average potential of mean force that includes contributions from both wet and dry states. When hydrodynamic interactions are considered (Avg-HI), the friction coefficient profiles depicted in Fig. 2 are utilized. In the case of no hydrodynamic interaction (Avg-NOHI) the diffusion constant $D_{\rm wet}$ is utilized for all values of q.

The spatial probability distribution at time $t,\,p(q,t)=\sum_s p(s,q,t)$ can be compiled from a set of molecular dynamics trajectories and compared to the results for the models that are obtained from the solution of Eq. 3. The probability distribution at t = 50 ps and t = 100 ps, is plotted in Fig. 4. It can be readily seen that the MD result exhibits three peaks: one corresponding to the basin in the mean force that is created by the wall potential at large separations, a smaller, more transient peak in the dewetting region, and a peak corresponding to ligand in the docked state. For long times, the distribution is localized in the docked pose, or in the case of the models based on Eq. (3), in the absorbing state.

Whereas all Master Equation models considered reproduce the features at the ligand far from the pocket and for the ligand in the docked pose, the peak resulting from drying fluctuations is not described by the average potential of mean force alone (which is strictly attractive in this region). The results for MD and the DSHM model are in good agreement in this region (see insets of Fig. 4), as the model captures the peak position and decay from t=50 ps to t=100 ps very well given the model's resolution.

The results for Avg-HI given in Fig. 4 also exhibit a peak in p(t) in the drying region, but it

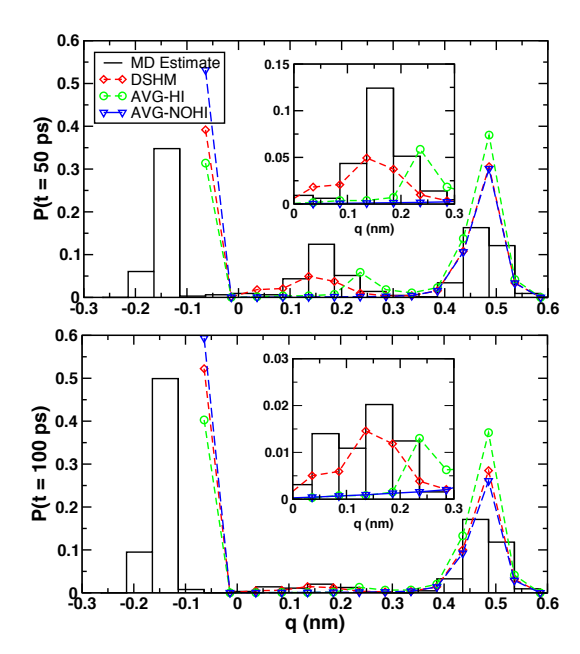


FIG. 4. Probability distribution of the assembly process at $t=50~\rm ps$ (top panel) and $t=100~\rm ps$ (bottom panel). The results from MD simulation (black bars) are compared against those extracted from three theories that can be expressed as Markovian master equations, one where the distribution evolves on two surfaces (DSHM, red line with diamonds), and where it evolves on an average surface with (AVG-HI) and without hydrodynamic interactions (AVG-NOHI) (green line with circles and blue line with triangles, respectively). Insets zoom into the distributions in the drying region.

is shifted with respect to the results of the MD and the DSHM. The peak in the Avg-HI distribution is shifted to the right of where the friction coefficient peaks and is related to where the smallest element of R_{ij} appears in the dewetting region (see the Appendix). From consideration of the DSHM, it is clear that this peak position is determined by the local minimum along the wet surface and that it is successful in reproducing the peak position present in the MD result. This shift in peak position is reminiscent of that reported in Ref. 17, where a difference was observed in the $\zeta(q)$ computed

from simulations in which q is restrained, and an effective spatial friction extracted from MFPT data. The authors attributed this shift to non-Markovian effects which we have seen are captured by DSHM.

The mean first passage times (MFPT) for assembly initiated from a wet state at $q_0=0.336$ nm are given in Table 2 for the models considered. It can be seen that, among all dynamical schemes presently considered, the MFPT obtained from DSHM comes closest to the results obtained from MD. The Avg-HI result significantly overestimates the MFPT. On the other hand the MFPT obtained from Avg-NOHI is a drastic underestimation of the result obtained from simulation, partly because it lacks a description of the drying transition.

In order to gain a more detailed understanding of the kinetics in the drying region, we compute the MFPT to assembly from initial wet configurations at pocket-ligand separations where the average surface points downhill towards assembly. Trajectories (about 3%) that recross into the region beyond the drying transition are not counted for the purpose of this calculation. The DSHM is in agreement with the results obtained from MD. As expected, the AVG-NOHI MFTP is far too low owing to its lack of a description of the drying phenomena. Interestingly, the AVG-HI model yields a reasonable result for one initial condition $(q_0 = 0.286 \text{ nm})$ but not the other $(q_0 = 0.186)$ nm). This result is another manifestation of the spatial shift of the probability distribution discussed above, such that the large hydrodynamic slowdown does not influence the (AVG-HI) results when the ligand is initially placed to the left of the center peak in Fig. 4.

IV. CONCLUSIONS

A full assessment of the kinetics of molecular recognition processes calls for the inclusion of molecular-scale hydrodynamic effects. However, most typically in coarse-grained models such effects are either ignored or treated within Markovian limit where the solvent time scales

are assumed to be fast compared to those of the heavy bodies. In reality, however slow solvent fluctuations are present when confined water molecules are expelled from the region between the ligand and the pocket wall. The non-Markovian nature of this problem begs for a more comprehensive theory which includes the solvent as an explicit part of the reaction path.

We present a simple model to study the kinetics of ligand binding in a model hydrophobic enclosure in conjunction with a novel coarsegrained theory for describing the solvent behavior in which solvent is accounted for by introducing a discrete state variable specifying whether the pocket is "dry" or "wet." In this way, diffusive motion along the (heavy body) assembly coordinate is coupled to transitions between the wet and dry surfaces. This model is found to yield an improved description of the assembly process when compared with models that ignore these state changes and obey standard Smoluchowski (Brownian) dynamics. In this way, the leading phenomena that give rise to non-Markovian behavior may be subsumed into a Markovian master equation description that lies in a larger state space.

Here we have explored the role of solvent in the kinetics of ligand-pocket association. Although our model is rather crude, it is still able to capture the displacement of water molecules by a ligand via hydrophobic drying transitions and the free energy barrier associated with ligand desolvation. However the ligand pocket is rather smooth and interactions are only mediated through the Lennard-Jones potential and not specific hydrogen bonding. Indeed, the presence of water may be more or less favorable near hetergeneous surfaces [28] or in different regions of the pocket [1]. Furthermore, the pocket and the ligand are both rigid structures in the simulations and the coupling of ligand and pocket internal degrees of freedom is not presently considered. Such effects may be rather slow and essential in the pathway to assembly, and may be incorporated in modified diffusive surface hopping models.

Assembly processes that occur in a bath of lighter particles are important in a wide vari-

		,	
	MFPT	MFPT	MFPT
	$q_0 = 0.336 \text{ nm}$	$q_0 = 0.286 \text{ nm}$	$q_0 = 0.186 \text{ nm}$
MD	473 ps	45 ps	42 ps
DSHM	351 ps	42 ps	34 ps
Avg-HI	816 ps	52 ps	5 ps
Avg-NOHI	193 ps	9 ps	3 ps

TABLE II. Mean first passage times (MFPT) as extracted from various models.

ety of settings. Molecular dynamics simulations provide an excellent tool for the study of such systems, although a deep understanding can be gained from the relation of large scale simulations to more coarse grained models of diffusion on smaller subsets of collective variables. This understanding can further clarify the kinetics of assembly processes and be incorporated into coarse-grained models. Future work will address this relation, as well as the behavior of patchy, softer, and more realistic bodies.

ACKNOWLEDGMENTS

This work was supported by grants from the National Institutes of Health [NIH-GM4330] and the National Science Foundation through [via Grant No. NSF-CHE-0910943]. We gratefully acknowledge the computational support of the Computational Center for Nanotechnology Innovations (CCNI) at Rensselaer Polytechnic Institute (RPI). This work used the Extreme Science and Engineering Discovery Environment

ronment (XSEDE), which is supported by National Science Foundation grant number OCI-1053575.

Appendix A: Expression for elements of dynamic matrix

The dynamics of a system that obeys a Markovian master equation description is given by Eq. 3 for the evolution of the probability distribution in state i, $p_i(t)$ In the two surface model, the index i runs over all allowed wet and dry states. The diffusive coordinate q is represented on a grid of spacing Δq . The matrix \mathbf{R} can be expressed as the sum of three matrices that describe distinct types of transitions,

$$\mathbf{R} = \mathbf{R}_d + \mathbf{R}_w + \mathbf{R}_{wd} \ . \tag{A1}$$

A diagram of this addition is shown in Fig. 5. The total dimension of \mathbf{R} is $N_w + N_d$. The matrices \mathbf{R}_d and \mathbf{R}_w describe transitions along q in the dry and wet states, respectively and have the following form:

$$R_s(q_i, q_j) = -\left[\omega_{+,j}^{(s)} + \omega_{-,j}^{(s)}\right] \delta_{ij} + \omega_{+,j}^{(s)} \delta_{j+1,j} + \omega_{-,j}^{(s)} \delta_{j-1,j}$$
(A2)

where 's' denotes either a wet or dry state and,

$$\omega_{+,n}^{(s)} = \frac{D(s, q_{n+1}) + D(s, q_n)}{2\Delta q^2} \exp(+\alpha)$$
(A3)

$$\omega_{-,n}^{(s)} = \frac{D(s, q_{n-1}) + D(s, q_n)}{2\Delta q^2} \exp(-\alpha) , \qquad (A4)$$

where,

$$\alpha = \frac{\beta \Delta q}{4} \left[\bar{F}(s, q_{n+1}) + \bar{F}(s, q_n) \right] . \tag{A5}$$

D and \bar{F} are the diffusion coefficient and mean force on a particular surface. These expressions represent a discretization of the Smoluchowski Equation (Eq. 1) [21].

In the Markovian (Brownian) limit, this expression along a single, averaged surface is considered. The spatial dependence in the diffusion coefficient engenders a maximum slowdown in the transition probability R_{ij} where the sum of the diffusion coefficients in states i and j is minimum. For the profile plotted in Fig. 2 this occurs at q = 0.236 nm, and is reflected in the peak position of p(q,t) that is observed in the AVG-HI model (Fig. 4). The peak position also can depend on \bar{F} , but it is roughly constant in the dewetting region on the average surface.

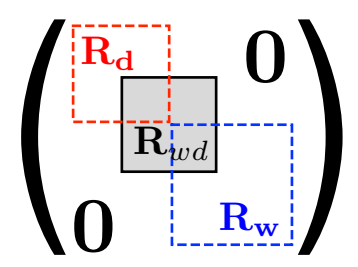


FIG. 5. A schematic of the addition of the matrices that comprise the rate matrix, \mathbf{R} . Transitions along q on the dry surface are described by \mathbf{R}_d , and along the wet surface by \mathbf{R}_w . \mathbf{R}_{wd} mediates transitions between the surfaces. The non-zero blocks of these matrices are denoted by the red, blue, and black boxes, respectively.

In the range of separations where wet-to-dry transitions may occur, they are described by the matrix \mathbf{R}_{wd} . If N_{wd} is the number of values of q for which such transitions are allowed, then the matrix is (square) block diagonal where the block has dimension of $2N_{wd}$. This block has diagonal elements: $-k(q, w \leftarrow d)$ for indices less than or equal to N_{wd} and $-k(q, d \leftarrow w)$ for indices greater than N_{wd} . The off diagonal components are non-zero for transitions between wet and dry states at the same value of q. The lifetime of the wet state is the inverse of the transition rates given in Table 1.

Appendix B: Simulation model and details

The model system in the current study, as depicted [19] in Fig. 6, is inspired by the one developed by McCammon and coworkers, [14] but with some distinct features, most notably that the size of the ligand and the pocket are larger, with a length scale on the order of 1 nm. In the present model, a semi-ellipsoidal (rather than hemispherical) pocket is "cut out" of a hexagonal close-packed (HCP) lattice. The equation for the ellipsoid is:

$$x^2 + y^2 + (cz)^2 = R^2$$
, (B1)

with c=0.8528 and R=1.1 nm. The pocket sites are fixed and interact with the model ligand with an Lennard-Jones potential with σ = 0.4152 nm, as in Ref [14]. The well depth is varied for the sites that line the pocket, as determined by a thickness of 0.17 nm. In this way, we vary the extent of hydrophobicity of the pocket. We have utilized three pocket types with different interaction potential well-depths: a) "highly attractive" interaction with ϵ =0.024 kJ/mol, b) "weakly attractive" interaction with ϵ =0.0024 kJ/mol and c) "intermediate attractive" interaction with ϵ =0.008 kJ/mol . All other pocket sites are assigned an $\epsilon = 0.0024$ kJ/mol as in Ref. 14. The main text concentrated on the case of intermediate attractive attraction (pocket ϵ =0.008 kJ/mol) and here, we elaborate on the other two parameter choices, namely the "highly attractive" and "weakly attractive" pocket.

Unlike in the work of McCammon and coworkers [14, 17] where a methane molecule was used to represent the ligand, we employ a nanoscale object in the form of C60 fullerene. This model of C60 fullerene has been utilized in one of our prior studies [12] and interacts with other bodies by means of a Lennard Jones potential with parameters ϵ =0.276 kJ/mol and σ =0.350 nm. The water is modeled with the TIP4P potential [29]. The solute-solvent inter-

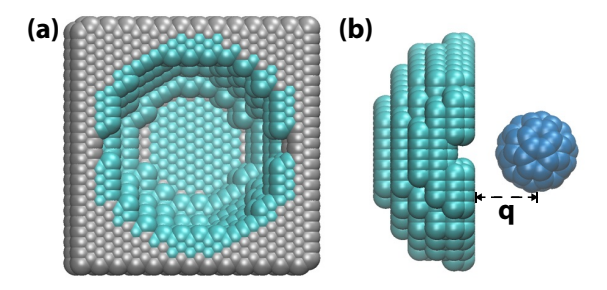


FIG. 6. Front and side view of the model ligand (C60 molecule, blue) and model pocket are depicted in panels (a) and (b), respectively. The well-depth associated with the LJ interaction (ϵ) of sites that line the pocket (green atoms) is varied in this study. Other sites (gray atoms) are assigned the smallest value of ϵ utilized in this work. The model is visualized with VMD.

actions are represented by the geometric mean of the respective water and solute parameters.

Appendix C: Technique to compute the hydrodynamic profile

In the Brownian limit, one can quantify the solvent-induced potential of mean force (PMF) and hydrodynamic profile between the pocket and ligand along a coordinate that is a function only of heavy-body positions. In the present work, this coordinate is along the direction of the difference between the center-of-masses of the pocket and the ligand and is zero where the ligand center of mass enters the cavity (see Fig. 6B)). This reaction coordinate, q, is only a function of the heavy bodies. The effect of the water is included implicitly through the induced potential of mean force experienced by the bodies and the hydrodynamic interactions encoded in the friction coefficient. The non-Markovian effects that arise from the slow solvent fluctuations are not treated by this framework, and the development of an alternative model (i.e. DSHM) is one of the chief aims of this study.

To calculate the solvent-induced potential of mean force, we utilize a similar protocol as in our prior work [12, 13]. A series of simulations are run keeping the pocket and ligand fixed at selected values of q. The ligand-pocket separation ranged from 0.86 nm to 2.46 nm at a separation of 0.1 nm and where needed, finer grid of spacing 0.05 nm was also used. The simulation box dimension, prior to equilibration, varied between 4.6 nm \times 4.6 nm \times 6.0 nm and 4.6 nm \times 4.6 nm \times 8.0 nm, depending on the pocketligand separation. Accordingly, the number of solvent molecules in the box also varied between 3375 and 4774. At each separation, the system was equilibrated under isothermal-isobaric (NPT) conditions for 1 ns and the data were collected in the canonical (NVT) ensemble for 5 ns. A stochastic velocity rescaling thermostat [30] was employed to maintain the temperature at 300 K for all simulations a Berendsen barostat [31] was employed at a pressure of 1 bar for constant pressure equilibration. The solventinduced mean force acting on the ligand and pocket are then computed from NVT runs at each separation. To obtain the solvent-induced potential of mean force (PMF), this quantity is then integrated along the reaction coordinate. Simulations were performed in the microcanconical (NVE) ensembles in order to evaluate the pocket-water fluctuations and solvent relaxation time. To maintain strict energy conservation in the microcanonical ensemble, NVE runs were performed in double precision. All simulations were performed using GROMACS 4.5.4 [32].

The position-dependent relative friction coefficient acting on the ligand as a function of pocket-ligand separation is computed in the following manner. In our recent work the friction coefficient was computed from the force-force autocorrelation function, [25] but in the present study we utilize an alternative method [26, 27] to compute the friction coefficient. In this method, one performs series of umbrella sampling simulations along the reaction coordinate and extracts the friction from the time correlation function of reaction coordinate po-

sition at a given separation:

$$\zeta(q) = k_b T \frac{\int dq \langle \delta q(t) \delta q(0) \rangle}{\langle \delta q^2 \rangle^2},$$
 (C1)

where $\delta q = q - \langle q \rangle$ represents the fluctuations of the reaction coordinate.

In our current study, the umbrella sampling technique is utilized instead of the force-force autocorrelation technique [25] that we previously employed [12, 13]. This is mainly due to the fact that the symmetries of the two-body friction tensor that are exploited in the work of Ref. 25 are not present when the two bodies are not identical as in the pocket-ligand complex.

The protocol for the friction calculation is as follows. The force constant of the umbrella potential was chosen such that it was the lowest value that engenders a Gaussian distribution about the average value of the reaction coordinate. The typical values of the force constant for the umbrella potential ranged between $3000 - 6000 \text{ kJ/mol/nm}^2$. At the ligand-pocket separation corresponding to the friction peak, we also repeated the calculation of the friction coefficient using different force constants. The uncertainties in the friction coefficient computed using different force constants was less than 10% of the average values. The following protocol was employed in order to compute position time correlation function to good statistical accuracy: At selected ligand-pocket separations, the system is first subjected to a short umbrella-sampling equilibration in the canonical (NVT) ensemble. Subsequently, microcanonical (NVE) umbrella sampling production runs were initiated by varying the initial velocity seeds. In the dewetting region, where very slow solvent fluctuations are present, twenty independent runs of up to 8 ns were carried out. Outside this region, it was found that ten, 4 ns long trajectories are sufficient to converge the results. The values of instantaneous reaction coordinates were collected every 0.01 ps from each run. To facilitate energy conservation, double precision routines and a smaller time step of 0.001 ps was utilized. Due to the expensive nature of the computation, the friction coefficient was computed at selected values of reaction coordinate. An estimate of the error in friction coefficient was also obtained by block averaging over multiple umbrella sampled trajectories for largest ligand-pocket separations as well as the ligand-pocket separation corresponding to friction peak. The uncertainty in the friction coefficient was 1-3% of the average values for the highly attractive and intermediate attractive cases and 1-15% of the average values for the weakly attractive cases.

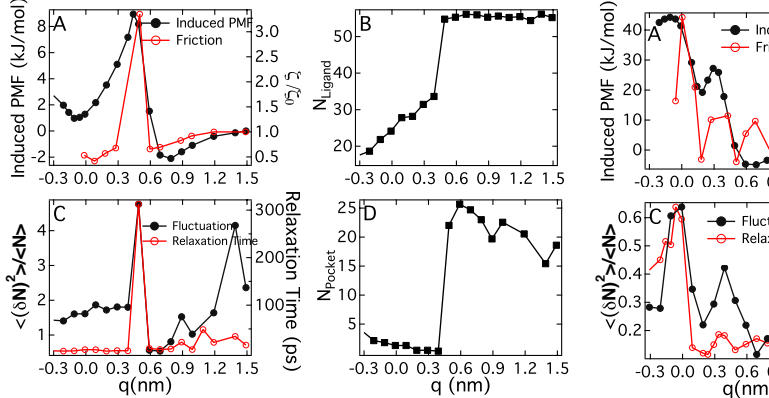
For the purpose of analysis, the variation of pocket-water and ligand-water as a function of distance are also computed. The 'ligand-water' is defined as the water in the first solvation shell ($R_{\rm CF-OW} < 0.8$ nm) of the ligand, and the 'pocket water' is simply the number of water molecules present in the pocket pocket (see Fig 6). The fluctuations and relaxation time of the pocket waters are computed at different ligand-pocket separations. The solvent fluctuations are given by the expression $\langle \delta N^2 \rangle / \langle N \rangle$ and the relaxation time by,

$$\tau = \frac{1}{\langle \delta N^2 \rangle} \int dt \, \langle \delta N(t) \delta N(0) \rangle , \qquad (C2)$$

where N is the number of water molecules in the pocket and $\delta N = N - \langle N \rangle$. In our previous work, such properties have been found to yield trends relatable to those observed for the profile of the friction coefficient [12, 13].

Appendix D: Hydrodynamics and solvent fluctuations in the hydrophilic and ideally hydrophobic cavities

The hydrodynamic profiles and the corresponding water-profile for the intermediate attractive pocket (ϵ =0.008 KJ/mol) have been discussed in the main text. In this Appendix, we will primarily discuss the results for the two remaining cases, namely the highly and weakly attractive pocket. In Figs. 7 and 8, we present pocket-water, ligand-water, the potential of mean force and variation of the frictional coefficient with separation for the ligand



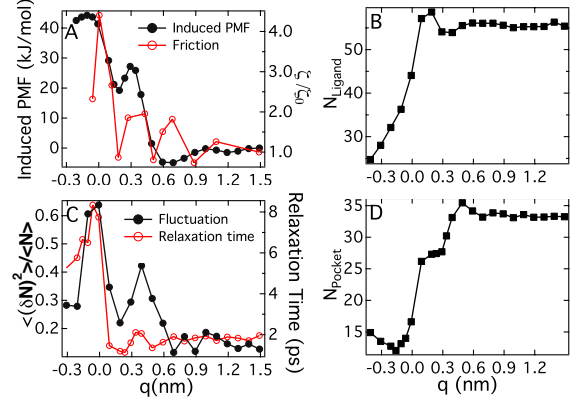


FIG. 7. Layout describing the correlations among various thermodynamic and hydrodynamic profiles as a function of ligand-pocket distance for weakly attractive pocket. (A) Comparison of the solvent-induced PMF (left scale) and frictional profile (right scale), (B) ligand-water number, (C) correlation of pocket-water fluctuation (left scale) and relaxation time (right scale), and (D) pocket-water number.

FIG. 8. Layout describing the correlations among various thermodynamic and hydrodynamic profiles as a function of ligand-pocket distance for highly attractive pocket. (A) Comparison of the solvent-induced PMF (left scale) and frictional profile (right scale), (B) ligand-water number profile, (C) correlation of pocket-water fluctuation (left scale) and relaxation time (right scale), and (D) pocket-water number profile.

interacting with the weakly and highly attractive pockets, respectively.

It can be seen that, even when the ligand is far away from the pocket (for large values of q), different water densities are present in all three pockets presently considered (see the main text for the pocket of intermediate attraction), owing to differences in the pocket hydration affinity. Naturally, as the C60 potential is not modified, the number of waters in the ligand solvation shell is the same at large q. As the ligand approaches the pocket, water is stripped from its solvation shell, and as it is rather hydrophilic, one can expect a contribution to the barrier to assembly arising from this process. There is an observed maximum in the number of pocket water as the ligand approaches the cavity, owing to the overlap of ligand solvation shell into the pocket.

When the ligand starts to enter the pocket ($\approx q = 0.5$ nm), the weakly attractive pocket undergoes a drying transition (see Fig. 7B). As in the case of intermediate attraction dis-

cussed in the main text, high friction coefficients and large and slow solvent fluctuations are associated with the drying transition, albeit at a larger pocket-ligand separation. The solventinduced free energy profile includes a relatively shallow basin at q = 0.8 nm and a barrier that is primarily engendered by the desolvation of the ligand. Hydrophobic attractive forces dominate and drive the ligand pocket complex to assembly, but there is an unexpected turnover of the free energy profile at very small pocket-ligand separations near the binding pose. We attribute this increase in the PMF for q < 0 to the retention of water brought in by the hydrophilic ligand, which is unfavorable in this hydrophobic pocket (see Fig 7D). We also note that even though most of these features in the solventinduced free energy profiles are also observed in the case of the pocket with intermediate attractions, the above-mentioned increase in free energy near the binding position is absent.

In the highly attractive pocket (Fig. 8), solvation water is stabilized by the relatively strong affinity of water for the cavity, even as the model ligand penetrates deeply into the pocket. Peaks in the friction correspond to features in the potential of mean force for q < 0.5 nm, as well as to large solvent fluctuations and relaxation times. The molecular-scale hydrodynamic effects are a manifestation of slow, confined water molecules which are "squeezed out" as the ligand is brought closer to the cavity wall. The highly attractive pocket expels water layer-bylayer as indicated by the decreases in number at q = 0.3 nm and q = 0. The difference in these separations is dictated by the diameter of the water molecule ($\sigma_{\rm O} \approx 0.3$ nm). As shown in our previous work [12, 13], the peaks in the friction can fortify the kinetic barriers to association that the ligand experiences as it traverses the free energy surface.

Appendix E: Further description of the Diffusive Surface Hopping Model

We propose a two dimensional model where one coordinate is the diffusive coordinate q (the separation between receptor and ligand), and the other is a discrete state variable s, indicating whether the binding pocket is wet or dry. As shown in the Eq. 2 in the main text, this model has state dependent diffusion constants D(s,q), evolves on state dependent free energy surfaces W(s,q), and its state can change from wet to dry and from dry to wet by first order kinetics with rate constants also depending on q. This model is equivalent to a particle diffusing on a potential energy surface that can hop between two functional forms, one for the wet and one for dry states, with different spatially dependent diffusion constants on each surface. We call this the Diffusive Surface Hopping Model (DSHM). The diffusion dynamics is thus coupled to transitions between the surfaces specified with rate constants $k(s \leftarrow s', q)$.

In our present model, 22 (9 dry and 13 wet) states are employed with a grid spacing of $\Delta q = 0.05$ nm to describe the system on the domain of -0.064 nm $\leq q \leq 0.636$ nm. For the purpose of this model, a state is defined as dry if there

are fewer than 15 water molecules in the pocket, and wet otherwise. The mean force is extracted from simulations where the ligand and pocket are fixed, and averages are taken separately over wet and dry states. The potentials of mean force corresponding to the wet and dry states are plotted in Fig. 3 in the main text. These surfaces include the direct interactions of the heavy bodies, which are strictly attractive on the domain of q that is currently considered. It can be seen that there is a relatively shallow minimum at $q \approx 0.15$ nm. The dry surface is strictly attractive and assembly proceeds readily after a transition to a dry state occurs. Transitions between the wet and dry surfaces are allowed in the region 0.036 nm $\leq q \leq$ 0.336 nm. The values of the transition rate constant at allowed values of q are given in Table 2 in the main text. Matrix elements for transitions, wet \rightleftharpoons dry, are estimated from the average dwell time in the dry state from MD simulations at fixed q. The transition times become shorter as the bodies approach each other and fewer water molecules are displaced by the drying event. In general, the dry state becomes more favorable at smaller separations. At q = 0.036 nm and q = 0.086nm, the transition rate parameters are estimated from the relaxation time of the solvent to irreversibly go from the wet to dry state, as wet states are not observed at long times.

In the drying region, the diffusion coefficient is approximated to be constant on each surface, albeit it is taken to be twice as large on the wet surface. This ratio is estimated from the position-position autocorrelation functions depicted in Fig. 3C of the main text. The value of the diffusion coefficient on the wet surface was taken to be equal to the diffusion coefficient at largest separations, $D_{\text{wet}} = 7.56 \times 10^{-4} \text{ nm}^2/\text{ps}.$ As the DSHM only explicitly describes the wet to dry transitions, other hydrodynamic effects, such as the confined nature of pocket water are not included, and therefore this value may be considered an upper bound on an appropriate estimate for D_{wet} . Outside the drying region, the diffusion coefficient is parameterized from the frictional profile (see Fig. 2A in the main text).

An absorbing boundary is set at q = -0.064 nm and a reflecting boundary is present at the wet state value of q = 0.036 nm. The former denotes a position where assembly is considered to occur and the latter choice is justified by the fact no wet states are allowed at smaller separations due to steric hinderance as observed from the highly attractive case.

Appendix F: Calculation of MFPT from MD simulations

In order to directly compare the dynamics of the Diffusive Surface Hopping Model to those of the explicit solvent molecular dynamics simulation and one dimensional Smoluchowski Dynamics, we study the time-dependent spatial distribution and the mean first passage times (MFPT) for assembly. For this purpose, we have carried out a separate set of MD simulations, where the pocket is fixed and the ligand is free to move in the direction of q. To guarantee that the ligand cannot diffuse far away from the binding site, a repulsive wall potential is added to the system. This is achieved by means of the PLUMED plugin for GROMACS [32, 33] and ensures that all configurations are bound to the domain q < 0.6 nm. The functional form of the boundary potential is as follows:

$$V_{\text{wall}}(q) = K(q - L)^4 \quad q \ge L$$

= 0 otherwise, (F1)

where $K = 15000 \text{ kJ/mol/nm}^4$ and L is the lower bound on q which is set at q = 0.366 nm (a position slightly to the right of barrier in the total PMF). With this boundary in place, the kinetics of assembly upon ligand entry into the pocket is described, but not the diffusion of the ligand up to the pocket entry. A total of 645 different ligand-binding trajectories were run, either by varying the velocity seeds or by changing the solvent configurations at a fixed initial condition, q_0 . The initial configuration for each run is always chosen such that the occupation of pocket waters corresponds to a wet state. If a dry state is chosen then assembly proceeds rapidly.

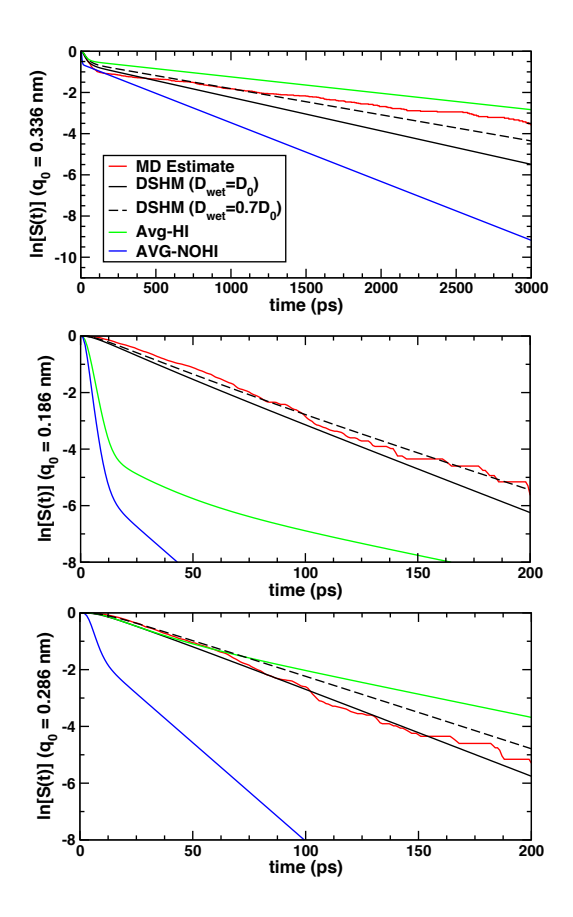


FIG. 9. The natural logarithm of the survival probability for the assembly process as estimated from a set of explicit solvent molecular dynamics trajectories (red curve) and coarse-grained models: the DSHM for two choices of the wet state diffusion coefficient (black curves), and Smoluchowski dynamics on the average surface with and without HI (green and blue curves, respectively). The data depicted in the top, center, and bottom panels correspond to the MFPTs presented in Table 2 of the main text at the corresponding initial states.

Appendix G: Survival probabilities: comparison of theory and MD

The Markovian master equation is given by the following expression,

$$\frac{\partial p_i(t)}{\partial t} = R_{ij}p_j(t) , \qquad (G1)$$

and has the following formal solution,

$$p_i(t) = T_{ij}(t)p_j(0) , \qquad (G2)$$

where the matrix \mathbf{T} is the propagator $e^{t \mathbf{R}}$. This exponentiated matrix may be readily evaluated in the eigenbasis of \mathbf{R} , which may be computed by means of standard linear algebra libraries. Given an absorbing state (at i=1), the survival probability may be computed from the sum over the probability of residing in non-absorbing states $S(t) = \sum_{i=2}^{N_w + N_d} p_i(t)$. The mean passage time is then obtained by taking the time integral of S(t).

The survival probability of assembly from $q_0 = 0.336$ nm is plotted in Fig. 9 on a log scale for the MD estimate as well as for the DSHM and Smoluchowski dynamics with and without hydrodynamic interactions (HI) on the average surface. It can be seen that although the DSHM exhibits reasonable agreement for the MFPT (see Table 2 of the main text), there are discrepancies at both short and long times. At short times, this is due to the fact that a larger fraction of MD trajectories initially proceed in the direction of assembly (67%) than predicted by the DSHM (54%).

At longer times, the disagreement can be alleviated by using a different choice for the diffusion coefficient on the wet surface in the drying region, D_{wet} . As discussed above, the value chosen is that of the diffusion coefficient at large separations (denoted as D_0 in Fig. 9) and can be considered an upper bound for this parameter. If D_{wet} is tuned so as to yield the same MFPT as the MD estimate, then D_{wet} is found to be approximately $0.7D_0$. This result is also plotted in Fig. 9, and this alteration is shown to improve agreement with the MD estimate at long times.

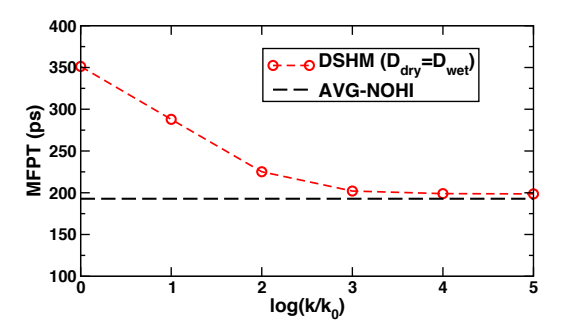


FIG. 10. The mean first passage time, is plotted for the DSHM as the dewetting transition rates, k, are increased for their baseline value, k_0 (red circles with dashed line). For very fast transitions, the results converge to the AVG-NOHI result (dashed black line), when the diffusion coefficient is taken to be $D_{\rm wet}$ on both surfaces.

In the middle and lower panels of Fig. 9, we plot the survival probably on a log scale that correspond to the passage through the dewetting region and whose integral corresponds to the MFPT values given the two right-hand columns of Table 2 in the main text. One can see how the Avg-HI model is far more sensitive to the change in initial position than the other schemes. The DSHM results exhibit some sensitivity to the choice of $D_{\rm wet}$, although overall agreement with the MD estimate is not greatly altered.

As the transition rate between wet and dry states increases, the resultant behavior should converge onto the result obtained from the average surface. This behavior arises from the fact that the Smoluchowski dynamics is recovered in the limit where the solvent dewetting fluctuations are fast. Our model is indeed able to produce this effect as is shown in Fig. 10. For the purpose of this result, we only consider a single diffusion constant on both the wet, dry, and average surfaces, $D_{\rm dry} = D_{\rm wet} = D_{\rm avg} = 7.56 \times 10^{-4} \ {\rm nm^2/ps}$. The initial distribution is again taken to be a wet state at $q_0 = 0.336$ nm. It can be clearly seen that, given the chosen parameters, as the transition rates are in-

- T. Young, R. Abel, B. Kim, B. J. Berne, and R. A. Friesner, Proc. Natl. Acad. Sci. USA 104, 808 (2007).
- [2] Y. Shan, E. T. Kim, M. P. Eastwood, R. O. Dror, M. A. Seeliger, and D. E. Shaw, J. Am. Chem. Soc. 133, 9181 (2011).
- [3] R. O. Dror, A. C. Pan, D. H. Arlow, D. W. Borhani, P. Maragakis, Y. Shan, H. Xu, and D. E. Shaw, Proc. Natl. Acad. Sci. USA 108, 13118 (2011).
- [4] R. A. Copeland, D. L. Pompliano, and T. D. Meek, Nature Reviews: Drug Discovery 5, 731 (2006).
- [5] B. J. Berne, J. Weeks, and R. Zhou, Ann. Rev. Phys. Chem. 60, 85 (2009).
- [6] J. C. Rasaiah, S. Garde, and G. Hummer, Ann. Rev. Phys. Chem. 59, 713 (2008).
- [7] D. Chandler, Nature **437**, 640 (2005).
- [8] S. Sharma and P. G. Debenedetti, Proc. Natl. Acad. Sci. USA 109, 4365 (2012).
- [9] S. Sharma and P. G. Debenedetti, J. Phys. Chem. B 116, 13282 (2012).
- [10] P. Liu, X. Huang, R. Zhou, and B. J. Berne, Nature 437, 159 (2005).
- [11] G. Hummer, J. C. Rasaiah, and J. Noworyta, Nature 414, 188 (2001).
- [12] J. A. Morrone, J. Li, and B. J. Berne, J. Phys. Chem. B 116, 378 (2012).
- [13] J. Li, J. A. Morrone, and B. J. Berne, J. Phys. Chem. B 116, 11537 (2012).
- [14] R. Baron, P. Setny, and J. A. McCammon, J. Am. Chem. Soc. 132, 12091 (2010).
- [15] R. Baron and J. A. McCammon, Annu. Rev. Phys. Chem. 64, 151 (2012).
- [16] J. C. Tully, J. Chem. Phys. 137, 22A301 (2012).
- [17] P. Setny, R. Baron, P. M. Kekenes-Huskey, J. A. McCammon, and J. Dzubiella, Proc. Natl. Acad. Sci. USA 110, 1197 (2013).

- [18] A. P. Willard and D. Chandler, J. Phys. Chem. B 112, 6187 (2008).
- [19] W. Humphrey, A. Dalke, and K. Schulten, J. Molec. Graphics 14, 33 (1996).
- [20] B. J. Berne and R. Pecora, Dynamic Light Scattering (Dover, 1990).
- [21] D. J. Bicout and A. Szabo, J. Chem. Phys. 109, 2325 (1998).
- [22] V. S. Pande, K. Beauchamp, and G. R. Bowman, Methods 52, 99 (2010).
- [23] S. Sriraman, I. G. Kevrekidis, and G. Hummer, J. Phys. Chem. B 109, 6479 (2005).
- [24] C. Gu, H. Chang, L. Maibaum, V. S. Pande, G. E. Carlsson, and L. J. Guibas, BMC Bioinformatics 14(Suppl 2), S8 (2013).
- [25] L. Bocquet, J. Hansen, and J. Piasecki, J. Stat. Phys. 89, 321 (1997).
- [26] J. E. Straub, B. J. Berne, and B. Roux, J. Chem. Phys. 93, 6804 (1990).
- [27] G. Hummer, New J. Phys. 7, 34 (2005).
- [28] N. Giovambattista, P. G. Debenedetti, and P. J. Rossky, J. Phys. Chem. C 111, 1323 (2007).
- [29] W. Jorgensen, J. Chandrasekhar, J. Madura, R. Impey, and M. Klein, J.Chem.Phys. 79, 926 (1983).
- [30] G. Bussi, D. Donadio, and M. Parrinello, J. Chem. Phys. 126, 014101 (2007).
- [31] H. J. C. Berendsen, J. P. M. Postma, W. F. van Gunsteren, A. DiNola, and J. R. Haak, J. Chem. Phys. 81, 3684 (1984).
- [32] B. Hess, C. Kutzner, and D. van der Spoel, J. Chem. Theor. Comput. 4, 435 (2008).
- [33] M. Bonomi, D. Branduardi, G. Bussi, C. Camilloni, D. Provasi, P. Raiteri, D. Donadio, F. Marinelli, F. Pietrucci, R. A. Broglia, and M. Parrinello, Comp. Phys. Comm. 180, 1961 (2009).